Abdominal Radiology (2022) 47:3645–3659
https://doi.org/10.1007/s00261-022-03625-y

PELVIS

Endorectal ultrasound radiomics in locally advanced rectal cancer patients: despeckling and radiotherapy response prediction using machine learning

Samira Abbaspour[1,2] · Hamid Abdollahi[3,8] · Hossein Arabalibeik[4] · Maedeh Barahman[5] · Amir Mohammad Arefpour[5] · Pedram Fadavi[6] · Mohammadreza Ay[1,2] · Seied Rabi Mahdavi[7]

Received: 13 March 2022 / Revised: 13 July 2022 / Accepted: 15 July 2022 / Published online: 11 August 2022

Abstract

Purpose The current study aimed to evaluate the association of endorectal ultrasound (EUS) radiomics features at different denoising filters based on machine learning algorithms and to predict radiotherapy response in locally advanced rectal cancer (LARC) patients.

Methods The EUS images of forty-three LARC patients, as a predictive biomarker for predicting the treatment response of neoadjuvant chemoradiotherapy (NCRT), were investigated. For despeckling, the EUS images were preprocessed by traditional filters (bilateral, wiener, lee, frost, median, and wavelet filters). The rectal tumors were delineated by two readers separately, and radiomics features were extracted. The least absolute shrinkage and selection operator were used for feature selection. Classifiers including logistic regression (LR), K-nearest neighbor (KNN), support vector machine (SVM), random forest, naive Bayes, and decision tree were trained using stratified fivefold cross-validation for model development. The area under the curve (AUC) of the receiver operating characteristic curve followed by accuracy, precision, sensitivity, and specificity were obtained for model performance assessment.

Results The wavelet filter had the best results with means of AUC: 0.83, accuracy: 77.41%, precision: 82.15%, and sensitivity: 79.41%. LR and SVM by having AUC: 0.71 and 0.76; accuracy: 70.0% and 71.5%; precision: 75.0% and 73.0%; sensitivity: 69.8% and 80.2%; and specificity: 70.0% and 60.9% had the highest model's performance, respectively.

Conclusion This study demonstrated that the EUS-based radiomics model could serve as pretreatment biomarkers in predicting pathologic features of rectal cancer. The wavelet filter and machine learning methods (LR and SVM) had good results on the EUS images of rectal cancer.

✉ Mohammadreza Ay
mohammadreza_ay@tums.ac.ir

✉ Seied Rabi Mahdavi
srmahdavi@hotmail.com

[1] Medical Physics and Biomedical Engineering Department, Faculty of Medicine, Tehran University of Medical Sciences, Tehran, Iran

[2] Research Center for Molecular and Cellular Imaging, Advanced Medical Technologies and Equipment Institute (AMTEI), Tehran University of Medical Sciences, Tehran, Iran

[3] Department of Radiology Technology, Faculty of Allied Medical Sciences, Kerman University of Medical Sciences, Kerman, Iran

[4] Research Center for Science and Technology in Medicine (RCSTM), Tehran University of Medical Sciences, Tehran, Iran

[5] Department of Radiation Oncology, Firoozgar Hospital, Firoozgar Clinical Research Development Center (FCRDC), Iran University of Medical Sciences, Tehran, Iran

[6] Department of Radiation Oncology, Iran University of Medical Sciences, Tehran, Iran

[7] Department of Medical Physics, School of Medicine, Iran University of Medical Sciences, Tehran, Iran

[8] Department of Integrative Oncology, BC Cancer Research Institute, Vancouver, Canada

Graphic abstract

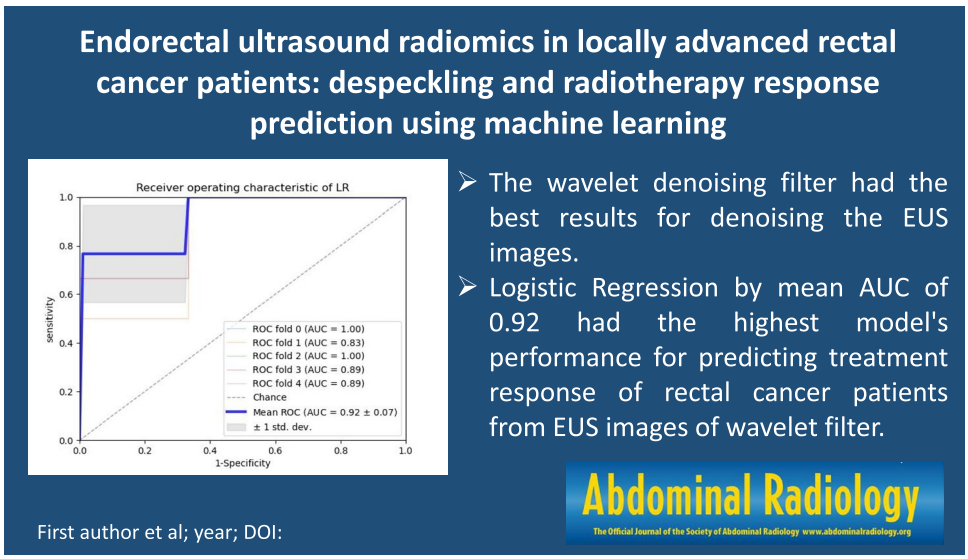

Keywords Denoising filters · Ultrasound · Rectal cancer · Treatment response · Radiomics features · Machine learning

Introduction

Rectal cancer/treatment

Rectal cancer accounts for one-third of the whole colorectal malignancies worldwide [1, 2]. Commonly, the method for treatment of locally advanced rectal cancer is neoadjuvant chemoradiotherapy (NCRT) followed by radical surgery, which causes a complete pathologic response (pCR) in 15% of patients [3]. This approach increased the chance of downstaging remarkably and reduced the risk of recurrence [4].

Techniques used for staging before surgery/EUS

Several methods are used for diagnosing/staging rectal cancer. Generally, techniques used for staging before surgery are included computed tomography (CT), ultrasound, magnetic resonance imaging (MRI), and positron emission tomography (PET) [5]. However, endorectal ultrasound (EUS) is an accurate modality for staging rectal cancer, and it is also a noninvasive, economical, radiation-free, and real-time method [6, 7].

Speckle/filters

One of the main factors affecting ultrasound images is speckle noise, which causes difficulty in visual observation [8, 9]. In other words, the speckle noise can degrade the fine details and edge definitions, as well as limit the contrast resolution in the ultrasound images [10]. The common classical filters used to despeckle images are detailed preserving anisotropic diffusion (DPAD), median, mean, wavelet, lee, frost, bilateral, and wiener filters [11, 12].

Radiomics/steps

Radiomics is a noninvasive helping tool to analyze biomedical imaging through quantitative features of the tumor or healthy tissues, which is not directly estimable visually [8]. The radiomics process involves image acquisition and preprocessing, the volume of interest segmentation, quantitative feature extraction, and feature reduction [13]. The selected features extracted from radiomics are used for several applications, such as therapy response prediction, accurate tumor characterization, and survival assessment [14–16].

US noise removal + radiomics

Using noise removal filters is one of the preprocessing methods for ultrasound image. The improved imaging can be entered into radiomics for further analysis. It has been reported that radiomics analysis based on ultrasound imaging has achieved several favorable results, especially in the early diagnosis, prognosis, and prediction of diseases [6].

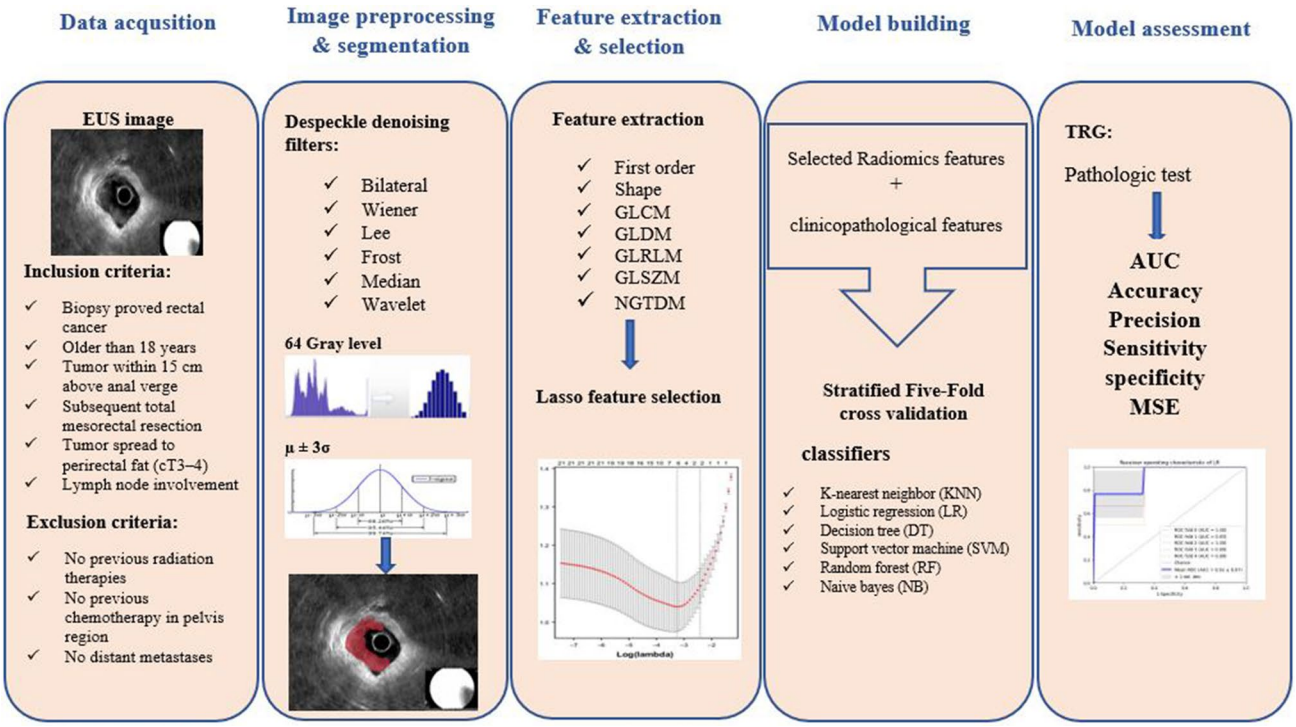

Fig. 1 Study flowchart

Filters reduce/remove US speckle noise/help preprocessing (review)

Several studies have reported that filters reduce/remove speckle noise and help preprocess ultrasound images [9, 12, 17–19]. For instance, Loizou et al. [20] assessed various despeckle filters for ultrasound images of the common carotid artery. The authors compared 10 different despeckle filters, including linear filter (DsFlsmv, DsFlsminsc), nonlinear filter (DsFkuwahara), wiener linear filter (DsFwiener), median filter (DsFmedian), hybrid median filter (DsFhmedian), geometric filter (DsFgf), anisotropic diffusion filter (DsFad, DsFsrad), and coherent nonlinear anisotropic diffusion filter (DsFnldif) in software based on texture features, objective image quality evaluation, and quantitative image quality metrics. In another study, Saoji and Sarode [18] investigated the speckle and rician noise reduction in ultrasound images using median and Gaussian filters. They have utilized Peak signal-to-noise ratio (PSNR) as a statistical quantity for assessing the image quality. In addition, Duron et al. [19] assessed the inter-slice radiomic feature repeatability in ultrasound imaging of the orbit. The impact of preprocessing was analyzed using intensity standardization (with or without outliers' removal on whole images, bounding boxes or regions of interest, and gray-level discretization).

Research gap

Recently, few studies have focused on radiomics in response to chemoradiotherapy (CRT) and prognosis in locally advanced rectal cancer. Additionally, most of those studies used MRI [21, 22], FDG-PET [23], and CT images [24]. Notably, the mentioned studies have not assessed the efficiency of the filters utilized for speckle noise reduction using radiomics model and machine learning. Moreover, it has not been reported whether radiomics features on the EUS images can predict patient treatment response in locally advanced rectal cancer patients. Thus, in the current study, we intended to evaluate the association of radiomics textural features of the EUS images with different denoising filters in predicting treatment response for rectal cancer patients using machine learning algorithms.

Materials and methods

Flowchart

A summary of the present study methods as the "study flowchart" is drawn in Fig. 1.

Data/ethics

This prospective study was approved by the National Ethical Committee with the registration number of IR.TUMS.MEDICINE.REC.1399.244. Sixty patients with pathologically diagnosed rectal cancer (adenocarcinoma) were included with the following criteria: older than 18 years, tumor located up to 15 cm from anal verge, subsequent total mesorectal resection, and tumor spread to perirectal fat (cT3–4) or lymph node involvement. In addition, the patients with previous radiation therapy and/or chemotherapy in the pelvis region and distant metastases based on the pathologic assessment were excluded from the study. Finally, forty-three patients have been conducted on the pretreatment EUS images and postoperative pathologic test. Informed consent was obtained from all participants.

Imaging unit/specs

The EUS images were performed using an ultrasonic endoscope device (EG-580 UR, Fujifilm, Tokyo, Japan) by radial array that produce a 360° image in a plane perpendicular to the long axis of the endoscope's insertion tube with an ultrasonic processor SU-1. The main characteristics of the device for performing the transrectal endosonographic are 7.5 MHz frequency, 140° field of view, 2.8-mm working channel, and 1250-mm working length. The B-mode images were obtained by a gastroenterologist expert in the field of oncology with ten years of experience. Rectal cancers can be observed on EUS images as hypoechoic masses which disrupt the normal five-layer structure of the rectal wall (mucosae, muscularis mucosae, submucosa, muscularis propria, and serosa). The physician captured about five images for each patient, and after that, the largest dimension of the tumor, as the best image, was chosen. It should be noted that the EUS examinations were carried out 1 week before CRT and 14 weeks before surgery.

Applied therapy

All patients were treated using three-dimensional conformal radiation therapy with a total dose of 45 Gy (dose fractionation: 1.8 Gy, 25 sessions) to the pelvic nodes, followed by a sequential boost of 5.4 Gy (1.8 Gy/day; total dose of 50.40 Gy). Furthermore, they were undergoing chemotherapy using capecitabine at a dose of 825 mg/m^2 orally, twice daily during radiation therapy days. Surgery (total mesorectal excision) was performed after 6–8 weeks of the mentioned procedures [3].

Grading

Treatment response based on the pathologic postoperative data was assessed according to the 4-category American

Table 1 Parameters of investigated filters

Filter	Parameters	Definition	References
Bilateral	Type: nonlinear, window size: 3*3, sigma_d:0.8, sigma_r:30	Smoothing images while preserving edges using a nonlinear combination of nearby image values	Vanithamani and Umamaheswari [26]
Wiener	Type: linear, window size: 3*3	Noise from image by comparing desired noiseless image would reduce by this technique. Wiener filter works on the basis of computation of local image variance	Jaybhay and Shastri [27]
Lee	Type: linear, window size: 3*3, iterations: 3	Based on the minimum mean square error. For removing speckle noise, this filter computes a linear combination of the center pixel intensity in a filter window with an average intensity of the window	Santoso et al. [28]
Frost	Type: linear, window size: 3*3, Damping factor: 1	Adaptive and exponentially weighted averaging filter based on the coefficient of variation and is derived from the minimum mean square error algorithm. It can suppress the speckle while at the same preserving the edges	Santoso et al. [28] and Kupidura [29]
Median	Type: nonlinear, window size: 3*3	Spatial nonlinear edge-preserving filter. The pixel of interest is replaced by the median value within the filter window	Santoso et al. [28], and Kupidura [29]
Wavelet	Type: discrete wavelet filtering, level: 2, wavelet name: Daubechies	Includes three steps: forward transformation of the image to the wavelet domain, reduction of the wavelet coefficients, and inverse transformation to the native domain	Mohd Sagheer and George [30]

Joint Committee on Cancer and College of American Pathologists (AJCC/CAP).

All samples were analyzed by one experienced pathologist and were further reviewed by a dedicated gastrointestinal pathologist using the modified tumor regression grade (TRG) to determine the pathologic response. Notably, the pathologists were blinded to the clinical data. The TRG was classified as follows: grade 0 (complete response) as no viable cancer cell; grade I (moderate response) single cells or small groups of cancer cells are visible; grade II (minimal response) is residual cancer outgrown by fibrosis; and grade III (poor response) is fibrosis outgrown by residual cancer. According to the results of pathologic grading, the patients were divided into two classes; the responder (grade 0 or grade I) as class 1 and/or non-responder (grade II or grade III) as class 0 [25].

Filters

To improve the visual quality, noise reduction is considered as a preprocessing step for further analysis, like image segmentation of the ultrasound images [20]. Several new ultrasound image filters are currently used for noise reduction [10]. In the current work, median, wavelet, lee, frost, bilateral, and wiener filters were used to reduce speckle noise (details of filters are described in Table 1). This study assessed the effects of the filters mentioned above on classification performance.

Performance evaluation—PSNR & SSIM

In addition, the performance of the filters was evaluated by MATLAB software (v.2019b), in terms of PSNR, which is the root mean square error (MSE) between noise free and denoised images (Eq. 1), and also the structural similarity index (SSIM), which measures the similarity between original and denoised images (Eq. 2).

$$10log_{10}\frac{255^2}{MSE}, \tag{1}$$

$$SSIM(x,y) = \frac{\left(2\mu_x\mu_y + c_1\right)\left(2\sigma_{xy} + c_2\right)}{\left(\mu^2{}_x + \mu^2{}_y + c_1\right)\left(\sigma^2{}_x + \sigma^2{}_y + c_2\right)}. \tag{2}$$

Here, μ_x, μ_y and σ_x, σ_y are the mean and standard deviations of the input and denoised images, in that order. σ_{xy} is the cross-covariance of the image. Notably, the applied method's performance is good when the PSNR value is high and the SSIM value is close to 1 [9].

Tumor segmentation

The EUS images were segmented using the open-source software package 3D slicer v. 4.10.2. One slice containing the largest dimension of the tumor was selected and then contoured by two physicians to manually place the region of interest (ROI) covering the rectal tumor. One physician was a radiologist specializing in rectal imaging with 5 years of experience; another was a radio-oncologist specializing in gastrointestinal cancer with 5 years of experience.

Radiomics features

The 102 radiomics features were extracted on EUS images using the "Pyradiomics" package (v3.0.1) in Python for each patient. The features consisted of first order, shape based, and textural features. Texture sets included gray-level run-length matrix (GLRLM), gray-level co-occurrence matrix (GLCM), gray-level size zone matrix (GLSZM), gray-level dependence matrix (GLDM), and neighboring gray tone difference matrix (NGTDM).

Need for FS—fivefold cross-validation

The 43 investigated patients were divided into the training and test sets using the stratified fivefold cross-validation method, independent of each other. After splitting, the models were built with the training data and evaluated with the test set to get the accuracy rate and other parameters, which help to compare the models and find the best classifier for the data. In stratified fivefold cross-validation, the partitions are selected in such a way that they all share the same balance between class labels (0, 1) [31–33].

Feature selection: AUC + LASSO

The feature reduction should be carried out because there is a risk of over-fitting analyses when the number of derived features becomes comparable to or exceeds the number of samples. The receiver operating characteristic (ROC) curve was calculated to assess the predictive power of the EUS features. The features with an AUC (area under the curve) of > 0.5 were considered high power. Then, to select useful predictive features, the least absolute shrinkage and selection operator (LASSO) method were applied for the training set [5]. In addition, the other clinical pathological and characteristics, including gender, age, pre-CRT T stage, pre-CRT N stage, tumor differentiation (well, moderate, poor), distance from the anal verge (cm), and length of tumor (cm) were assessed.

Table 2 The patient characteristics, clinicopathological information, and pathologic response of rectal cancer

Characteristic	All patients ($n=43$)	Training set ($n=34$)	Test set ($n=9$)
Gender			
Male	28	23	5
Female	15	11	4
Age (years) Mean ± SD (range)			
Male	60 ± 12.5 (39–81)	61 ± 11 (29–80)	59 ± 13 (31–79)
Female	58 ± 12.5 (31–80)	60 ± 12 (32–80)	56 ± 11 (35–77)
T stage			
T1	2	1	1
T2	5	3	2
T3	26	22	4
T4	10	8	2
N stage			
N0	6	4	2
N1	12	10	2
N2	25	20	5
Pathologic differentiation			
Well	12	9	3
Moderate	22	18	4
Poor	9	7	2
Distance from anal verge (cm)			
Low rectal cancer (0–6 cm)	21	16	5
Middle rectal cancer (6–12 cm)	14	11	3
High rectal cancer (> 12 cm)	8	7	1
Response to NCRT			
TRG = 0	7	5	2
TRG = 1	11	8	3
TRG = 2	21	18	3
TRG = 3	4	3	1

Classifiers + prediction power evaluation

The selected features as covariates (X) and the pathology results of the rectal cancer as a dependent variable (Y) were used in K-nearest neighbor (KNN), support vector machine (SVM), logistic regression (LR), decision tree (DT), random forest (RF), and naive Bayes (NB) methods to build a prediction model. Additionally, the independent test set was utilized to evaluate the performance of the model. The machine learning algorithms were implemented on Python's "scikit-learn" package (v 0.24.2). The power of the mentioned models for predicting therapeutic response was calculated using the following parameters: AUC, accuracy, precision, sensitivity, specificity, and MSE.

Gold-standard evaluation

Intraclass correlation coefficient (ICC) with the 95% confidence interval (CI) was utilized for interobserver agreement. ICC was evaluated based on a two-way random effect model among the investigated features. Equation 3 is used for the ICC calculation [14, 34]:

$$ICC = \frac{MS_R - MS_W}{MS_R + (k-1)MS_W}, \quad (3)$$

where MS_R defines "the mean square for rows, each feature value for the two observers," MS_W indicates "the mean square for the residual source of variance," k relates to the number of the observers, and n is the number of subjects.

The R package (v. 1.4.1106) was used for ICC computations. The P values of less than 0.05 were considered statistically significant.

Results

Patient characteristics

The patient demographic and clinicopathological information and also the results related to the pathologic response

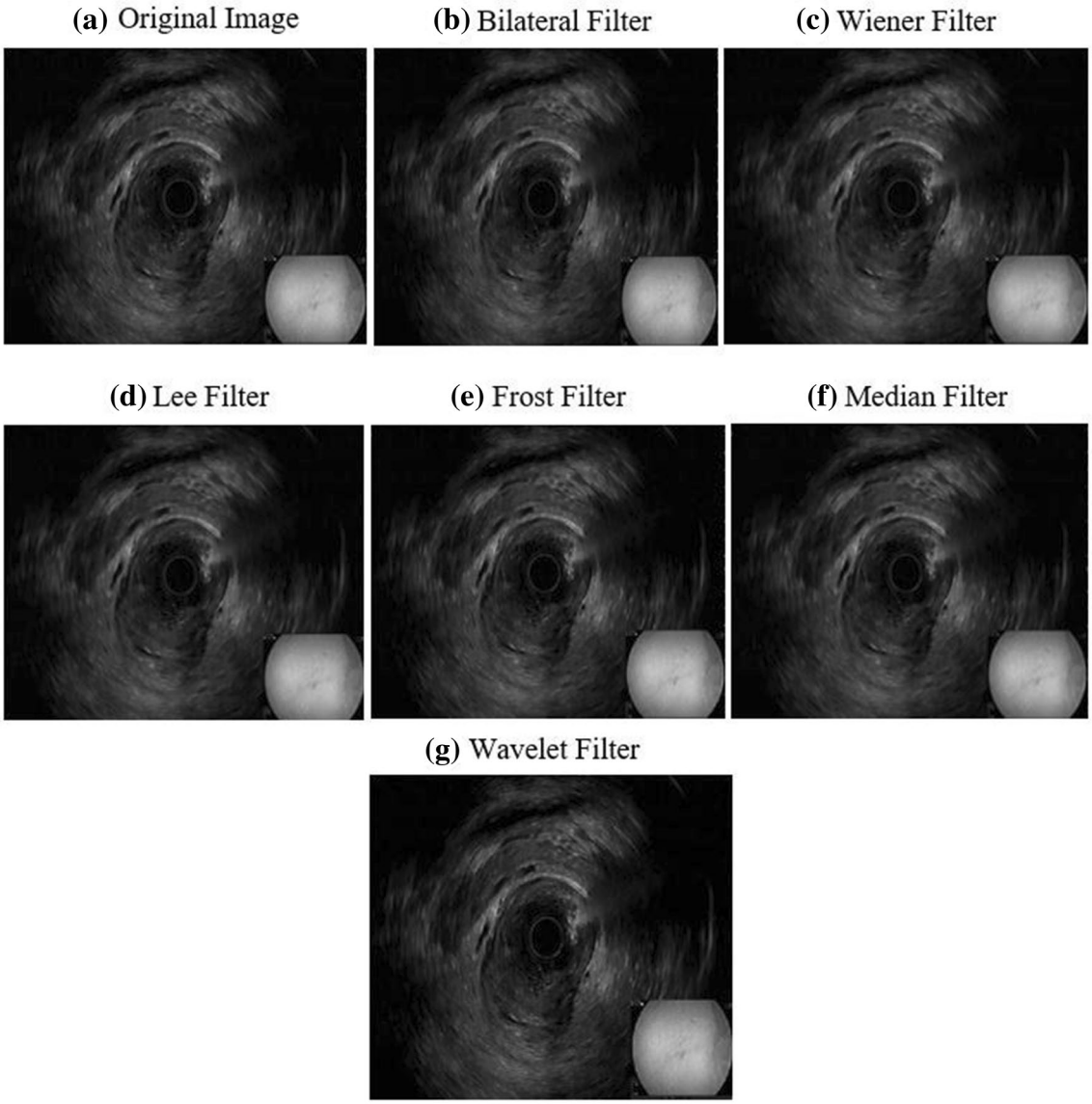

Fig. 2 The proposed denoising filters for a sample image, **a** Original image, **b** Bilateral filter, **c** Wiener filter, **d** Lee filter, **e** Frost filter, **f** Median filter, and **g** Wavelet filter. To the eye, these images do not look very different from each other, and the major difference is the quantity value (radiomics feature values)

of rectal cancer are presented in Table 2. As depicted, eighteen patients were classified as responders and twenty-five were non-responders. The training and test dataset showed a reasonable distribution between the pCR rate and clinicopathological features.

Filter outputs + final selected features

A sample of the EUS image along with the output of each filter (bilateral, wiener, lee, frost, median, and wavelet) used for speckle noise removal is shown in Fig. 2. For each filter output, 102 features were extracted from the delineated target volume and categorized as follows: shape (9 features), first order (18 features), and texture (24 GLCM, 14 GLDM, 16 GLRLM, 16 GLSZM, and 5 NGTDM features) (Supplementary 1). The selected features (using LASSO method) as the most significant features for the original image and each filter output are shown in Fig. 3.

Prediction results

The clinicopathological predictors were added to the selected discriminative radiomics features and then a EUS radiomics predictive model was developed using machine learning models.

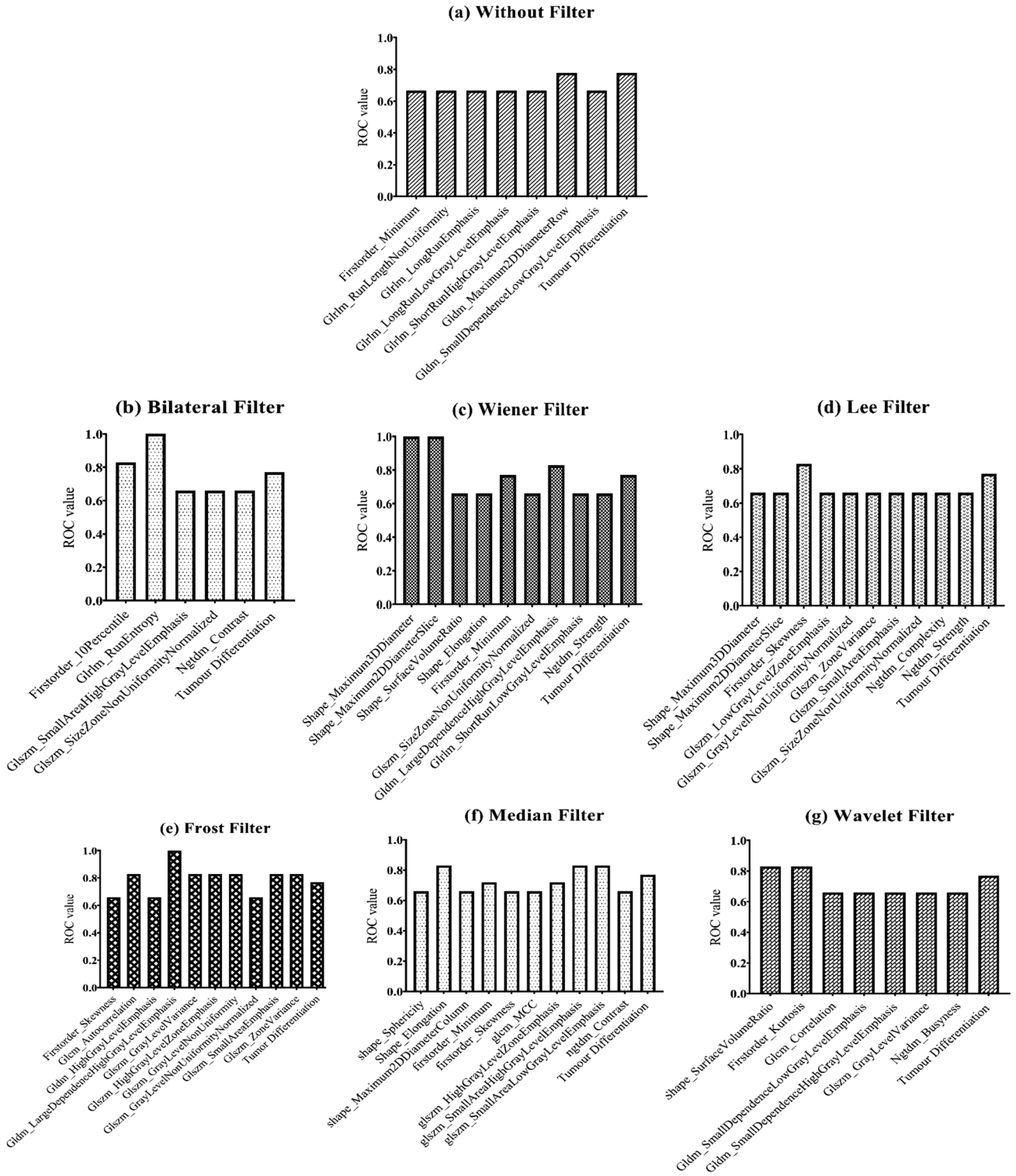

Fig. 3 The selected features using LASSO model via stratified fivefold cross-validation in filtered images

The predictive ability metrics for each model (KNN, LR, SVM, DT, RF, and NB) are depicted in Table 3. According to Table 3, the SVM classifier provided the best capability to predict patients response to NCRT with the average AUC of 0.76 (accuracy: 71.5%; precision: 73.0%; sensitivity: 80.2%; and specificity: 60.9%). Moreover, the LR classifier showed a good performance with the average AUC of 0.71 (accuracy: 70.0%; precision: 75.0%; sensitivity: 69.8%; and

Table 3 Performance assessment for the investigated models and filters in train and test data

Filters	Model	AUC		Accuracy		Precision		Sensitivity		Specificity		MSE	
		Train	Test	Train	Test	Train	Test	Train	Test	Train	Test	Train	Test
Original	KNN	0.31	0.26	0.78	0.642	0.834	0.71	0.775	0.716	0.783	0.533	0.219	0.357
	LR	0.75	0.64	0.666	0.638	0.896	0.773	0.443	0.61	0.933	0.66	0.333	0.361
	DT	0.83	0.508	0.825	0.514	0.896	0.5	0.778	0.483	0.883	0.533	0.174	0.485
	SVM	0.81	0.6	0.734	0.614	0.754	0.69	0.761	0.66	0.7	0.533	0.265	0.385
	NB	0.82	0.65	0.72	0.576	0.748	0.613	0.737	0.6	0.7	0.533	0.279	0.423
	RF	0.86	0.483	0.856	0.485	0.912	0.433	0.821	0.433	0.9	0.533	0.14	0.51
Bilateral	KNN	0.81	0.65	0.765	0.619	0.852	0.653	0.693	0.683	0.85	0.533	0.234	0.380
	LR	0.85	0.66	0.764	0.633	0.753	0.703	0.846	0.66	0.66	0.6	0.235	0.366
	DT	0.88	0.541	0.871	0.538	0.973	0.623	0.793	0.616	0.966	0.466	0.128	0.461
	SVM	0.76	0.75	0.848	0.695	0.869	0.716	0.860	0.783	0.833	0.6	0.151	0.304
	NB	0.81	0.8	0.750	0.661	0.810	0.763	0.708	0.683	0.8	0.66	0.249	0.338
	RF	0.906	0.508	0.901	0.49	0.97	0.573	0.889	0.5	0.966	0.533	0.075	0.49
Wiener	KNN	0.87	0.63	0.801	0.685	0.893	0.693	0.72	0.75	0.9	0.6	0.198	0.314
	LR	0.88	0.79	0.817	0.785	0.814	0.809	0.860	0.833	0.766	0.733	0.182	0.214
	DT	0.94	0.483	0.939	0.485	0.957	0.533	0.93	0.433	0.95	0.533	0.06	0.514
	SVM	0.78	0.76	0.885	0.661	0.889	0.730	0.900	0.7	0.866	0.6	0.114	0.338
	NB	0.82	0.72	0.719	0.695	0.971	0.933	0.5	0.5	0.983	0.933	0.280	0.304
	RF	0.93	0.658	0.932	0.66	0.934	0.68	0.944	0.71	0.916	0.6	0.067	0.33
Lee	KNN	0.8	0.58	0.690	0.576	0.685	0.570	0.793	0.733	0.566	0.399	0.309	0.423
	LR	0.91	0.7	0.849	0.761	0.874	0.783	0.848	0.783	0.85	0.733	0.150	0.238
	DT	0.903	0.558	0.901	0.547	0.938	0.553	0.889	0.45	0.916	0.66	0.098	0.452
	SVM	0.95	0.64	0.879	0.671	0.852	0.653	0.944	0.8	0.8	0.533	0.12	0.328
	NB	0.83	0.71	0.734	0.576	0.761	0.603	0.747	0.616	0.716	0.533	0.265	0.423
	RF	0.886	0.583	0.880	0.588	0.869	0.606	0.943	0.7	0.816	0.466	0.113	0.419
Frost	KNN	0.84	0.51	0.803	0.538	0.804	0.546	0.848	0.583	0.75	0.466	0.196	0.461
	LR	0.85	0.54	0.788	0.485	0.792	0.533	0.834	0.45	0.733	0.533	0.211	0.514
	DT	0.859	0.583	0.854	0.576	0.923	0.683	0.801	0.566	0.916	0.6	0.145	0.423
	SVM	0.76	0.67	0.849	0.666	0.819	0.65	0.931	0.833	0.75	0.466	0.150	0.333
	NB	0.79	0.58	0.621	0.547	0.826	0.733	0.390	0.333	0.9	0.799	0.378	0.452
	RF	0.889	0.6	0.893	0.609	0.885	0.67	0.929	0.733	0.85	0.466	0.1	0.39
Median	KNN	0.92	0.82	0.863	0.752	0.898	0.843	0.847	0.7	0.883	0.799	0.136	0.247
	LR	0.89	0.65	0.863	0.676	0.896	0.766	0.847	0.633	0.883	0.733	0.136	0.323
	DT	0.919	0.641	0.917	0.64	0.943	0.703	0.904	0.616	0.933	0.66	0.082	0.357
	SVM	0.99	0.86	0.954	0.752	0.958	0.77	0.958	0.816	0.95	0.66	0.045	0.247
	NB	0.89	0.68	0.795	0.661	0.882	0.85	0.720	0.55	0.883	0.8	0.204	0.338
	RF	0.939	0.608	0.939	0.609	0.948	0.69	0.944	0.616	0.933	0.6	0.105	0.35
Wavelet	KNN	0.93	0.89	0.878	0.819	0.922	0.86	0.846	0.833	0.916	0.799	0.121	0.180
	LR	**0.98**	**0.92**	**0.909**	**0.847**	**0.955**	**0.9**	**0.874**	**0.833**	**0.95**	**0.866**	**0.090**	**0.152**
	DT	0.938	0.675	0.938	0.671	0.944	0.74	0.943	0.75	0.943	0.6	0.061	0.328
	SVM	**0.98**	**0.9**	**0.931**	**0.847**	**0.944**	**0.86**	**0.930**	**0.883**	**0.933**	**0.799**	**0.068**	**0.152**
	NB	0.92	0.89	0.871	0.761	0.913	0.826	0.846	0.733	0.9	0.799	0.128	0.238
	RF	0.945	0.7	0.947	0.7	0.945	0.743	0.958	0.733	0.933	0.66	0.052	0.295

The LR and SVM models from the wavelet filter had the best results

specificity: 70.0%). In addition, the training accuracy was remarkably increased than the testing accuracy indicating the investigated models were overfit for treatment response predictions. This can be due to the too small events number to generate a stable model. Figure 4 shows ROC of LR and SVM models for the original image and wavelet filter output in test data.

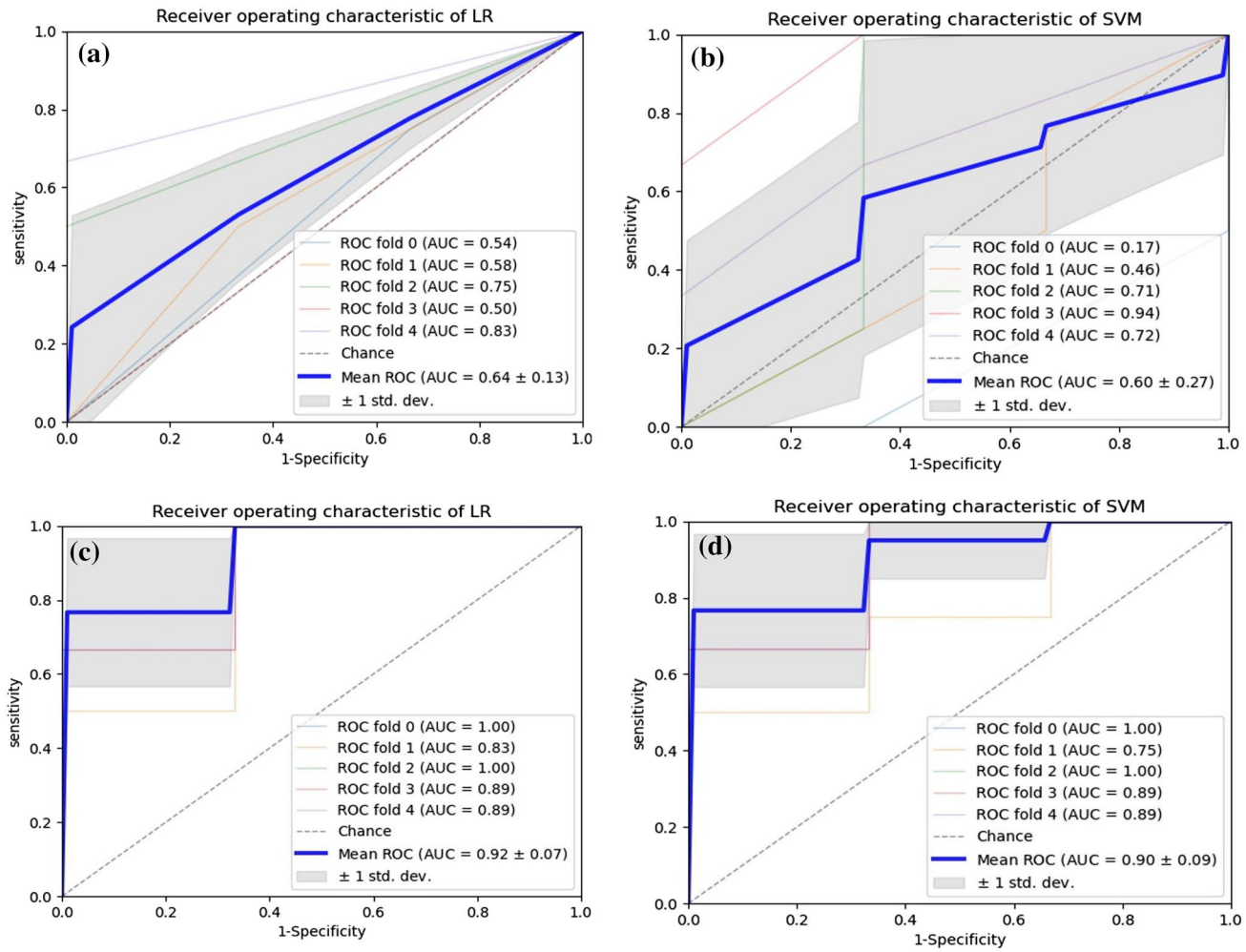

Fig. 4 ROC curve **a** LR model for the original image, **b** SVM model for the original image, **c** LR model for the filtered by wavelet, and **d** SVM model for the filtered by wavelet in the test data

Denoising results

The average results of the denoising filters according to PSNR and SSIM metrics are presented in Table 4. It can be seen that PSNR and SSIM for the wavelet filter are 40.02 and 0.96, respectively. The correlation between the selected features of the wavelet filter is shown in Fig. 5. As can be seen, Gldm_SmallDependenceHighGrayLevelEmphasis is highly correlated with Glszm_GrayLevelVariance and Gldm_SmallDependenceLowGrayLevelEmphasis (correlation coefficients > 0.8).

Based on the machine learning results, PSNR, and SSIM values, the wavelet filter had the best performance (speckle noise reduction) chosen for image preprocessing.

Table 4 Average results of denoising algorithms

Denoising filters	PSNR	SSIM
Bilateral	31.04	0.95
Wiener	38.54	0.95
Lee	33.72	0.94
Frost	30.52	0.93
Median	29.58	0.92
Wavelet	40.02	0.96

Experts' correlation/agreement

The ICC of the extracted features between the two physicians ranged from 0.7 to 0.92. Figure 6 shows the ICC for the selected features extracted from the original image and different denoising filters. According to this Figure, there was a good agreement between the two observers with ICC higher than 0.7. Due to the different segmentations of images between physicians, the lowest limit of ICC values was found for shape features (0.7).

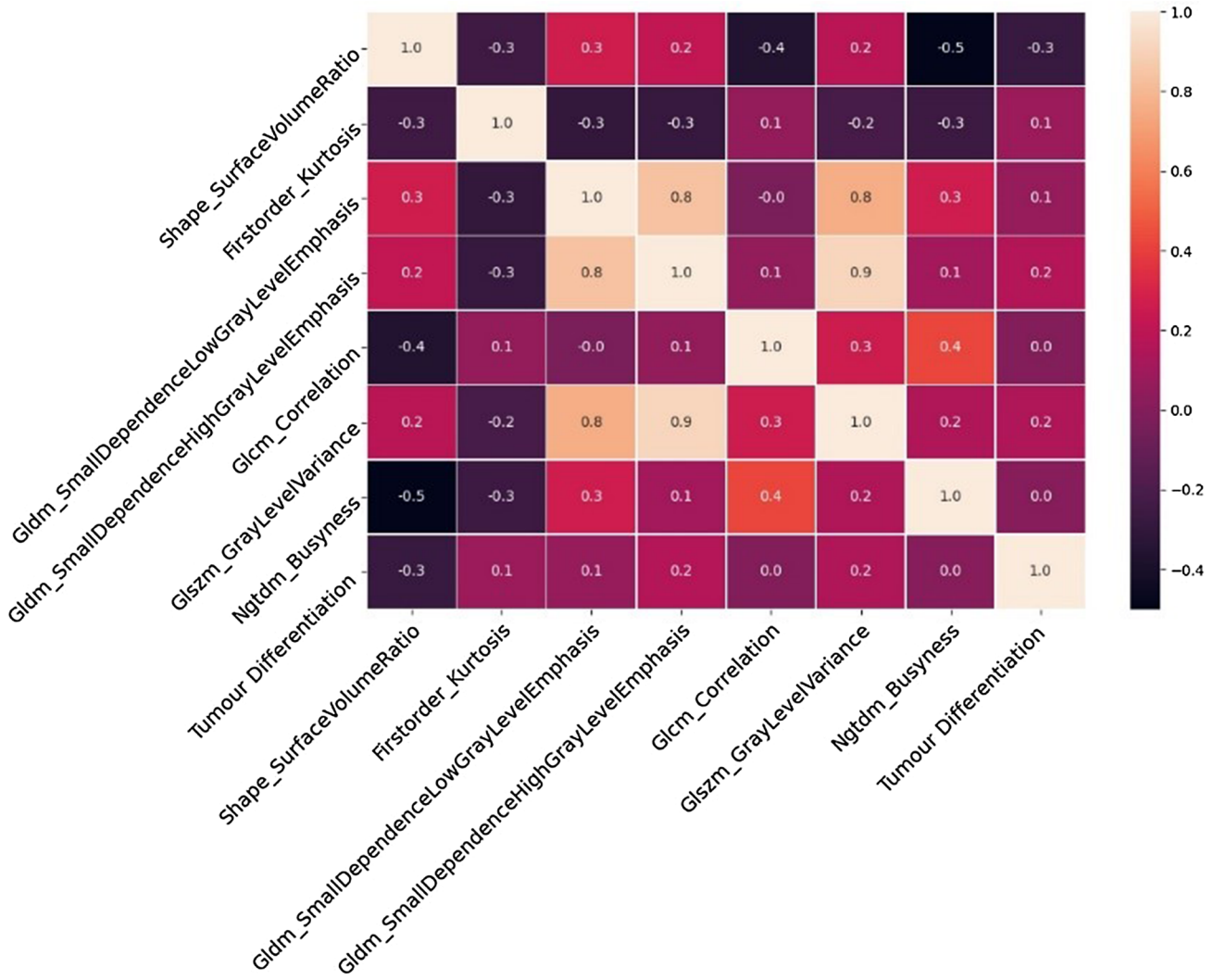

Fig. 5 Heatmap of the selected best radiomics features from the wavelet filter output

Discussion

The main clinical challenge in rectal cancer is the preoperative diagnosis of complete pathologic response in patients with LARC after NCRT. Commonly, specimens resected surgically are histopathologically examined and analyzed by experienced pathologists; pCR is defined as the absence of viable tumor cells in the primary tumor and lymph nodes [35]. In this scenario, radiomics has emerged as a promising tool that may serve as an imaging biomarker for tumor response [36]. This technique is used for clinical application to promote structured generation and application of qualitative and quantitative cancer treatment information [35, 37]. The image acquisition, preprocessing, segmentation of ROIs, feature extraction, and modeling are involved during the radiomics process [38].

This study assessed the feasibility of predicting outcomes for 43 rectal cancer patients using radiomics features extracted from the EUS images to identify patients with pCR and non-pCR. Hopefully, the results can provide additional information to decide whether to implement the watch-and-wait strategy for low-risk patients, in order to improve their quality of life. Furthermore, early detection of non-NCRT responders would facilitate physicians' decision-making to find alternative methods, such as targeted therapy and immunotherapy [39].

EUS and MRI as non-ionization radiation modalities can be used as complementary methods in the preoperative staging of rectal cancer. Compared to MRI, EUS is more accurate in determining rectal wall penetration of the tumor, which is also a more cost effective, fast, convenient, accessible, and safe method [5, 6]. However, the quality of ultrasound images is highly dependent on interobserver

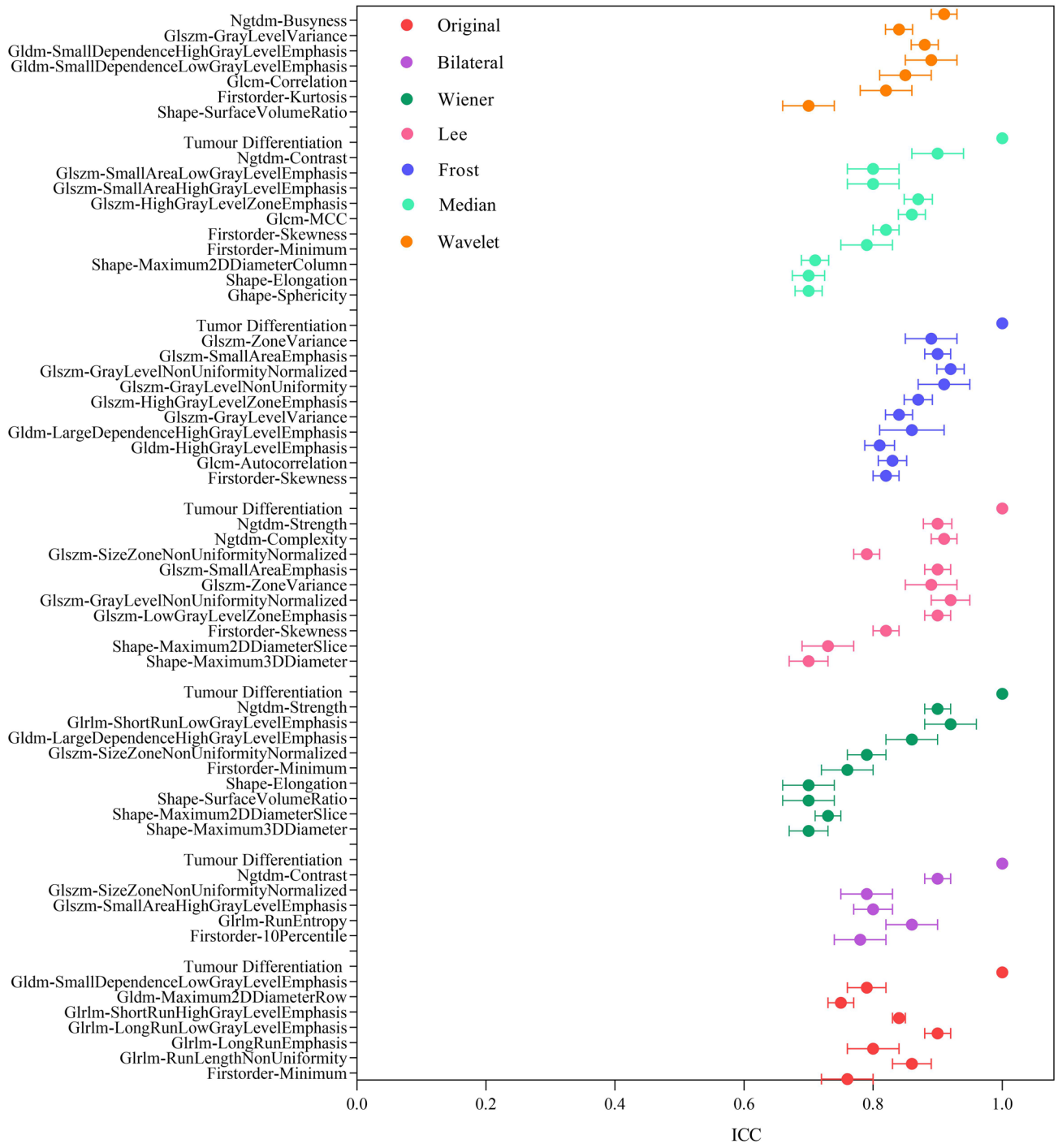

Fig. 6 Intraclass correlation coefficients of the two observers for the selected features extracted from the original and different denoising filters

variability, the abundance and experience of operators or diagnosticians, as well as different institutes, and manufacturers [40]. Ultrasound also presents unique challenges, including noise and artifacts that cause analysis difficulty, especially behind bone and air. Texture features and quality of the images, which carry out important information related to the tissues and organs [20], are affected by speckle noise [11, 12]. Thus, speckle noise reduction is a crucial research subject in ultrasound image processing. The two main purposes for speckle noise reduction are to improve human interpretation and despeckling, which are the preprocessing steps for many ultrasound image analyses [12]. Moreover, to increase the image detail, quality, and diagnostic accuracy, preprocessing is a crucial step performed

by different traditional filters in the current study [25]. All in all, the results of the current study and other investigations that used ultrasound in other organs, such as the breast and thyroid [41–45], show that radiomic analysis can be successfully performed on ultrasound data and helped render ultrasound-based tumor imaging more accurate, reproducible, and reliable.

In a study, Karaoğlu et al. [9] compared deep learning (WIN5-RB, DPDNN, and FPD-MNet), block-matching and 3D filtering (BM3D), and classical filters (bilateral, frost, kuan, lee, mean, and median) for speckle denoising. They have expressed that, although the performances of the deep learning were superior for despeckling ultrasound image noise compared to BM3D and classical filters in terms of PSNR and SSIM criteria, this method needs more time for training. In addition, in high-resolution images, deep learning performed better denoising; however, it is only possible with high computational capacity. For these reasons, we have used the six denoising traditional filters (bilateral, wiener, lee, frost, median, and wavelet filters) and their effects on radiomics features for reducing the ultrasound speckle noise.

The present work identified 8, 6, 10, 11, 11, 11, and 8 significant features including shape, first order, and texture features for predicting pCR versus non-pCR, from the original image, bilateral, wiener, lee, frost, median, and wavelet filters, respectively. Most importantly, we found that the best predictor features for pCR and non-pCR were based on the wavelet filter. In summary, the wavelet filter tends to give good results for all three metrics (radiomics, PSNR, and SSIM). This is the transform domain technique because the image is first converted into a wavelet domain and then the despeckling operation is performed by utilizing the different properties of the image. Several properties of the wavelet transform that make this representation attractive for denoising are multiresolution, edge detection, and edge clustering, as expressed in the previous studies [41–43,46,47].

The 8 features from the wavelet filter include Shape_SurfaceVolumeRatio, Firstorder_Kurtosis, Glcm_Correlation, Gldm_SmallDependenceLowGrayLevelEmphasis, Gldm_SmallDependenceHighGrayLevelEmphasis, Glszm_GrayLevelVariance, Ngtdm_Busyness, and Tumor Differentiation, which are of great value in accurately to identify the treatment response. Chen et al. [5] integrated EUS image features of rectal cancer for predicting tumor deposits preoperatively. In their study, MinIntensity, HaralickCorrelation_AllDirection_offset6_SD, and HaralickCorrelation_AllDirection_offset9_SD features were associated with tumor deposits. In another study, Theek et al. [48] assessed whether a radiomic analysis on contrast-enhanced ultrasound data allows to automatically differentiate three tumor models in an animal study. The selected radiomic features associated with tumor phenotypes included Median Image Intensity, Energy of Gray-Level Co-Occurrence Matrix, Vessel Network Length, and Run-Length Nonuniformity of the Gray-Level Run-Length Matrix. Based on these findings, it can be concluded that there are different image biomarkers for different organs and clinical results because of the various biological mechanisms behind the processes.

Owing to the results, LR and SVM models had the best performance among the six different investigated machine learning methods, and the wavelet filter indicated a reasonable result in these mentioned models. Several studies have used machine learning methods to analyze different modalities' images and defined/introduced the best model/models. For instance, Shayesteh et al. [49] investigated the performance of individual and ensemble machine learning models in rectal cancer patients based on MR imaging to predict NCRT response. The investigated models included SVM, Bayesian network, neural network, and KNN classifiers used individually and together. The best result was related to Bayesian network model with the AUC and accuracy of 75.2% and 80.9%, respectively. The AUC and accuracy values in the ensemble model were obtained at 97.8% and 92.8% in the testing set, respectively. Moreover, Ma et al. [13] demonstrated that the SVM model had better results (AUC: 0.862), in predicting tumor pathologic features of rectal cancer when they investigated MRI-based radiomics model derived from T2-weighted images. Dasgupta et al. [45] investigated quantitative ultrasound based on higher-order texture derivatives in predicting the response to NCRT in patients with locally advanced breast cancer. To develop radiomics models of response prediction, three machine learning algorithms based on linear discriminant (FLD), KNN, and SVM were used. A KNN model provided the best results with the sensitivity, specificity, accuracy, and AUC of 87%, 81%, 82%, and 0.86, in that order. These controversies may be attributed to several factors: various imaging modalities, the image acquisition machine and parameters, image preprocessing algorithm, image segmentation, tumor regions, and feature selection algorithms [24]. In addition, no ML method is better than any other for all problems. Our results show that LR and SVM models with an accuracy of 70.0% and 71.5% can be used for EUS images before CRT, respectively. Secondly, the wavelet filter should be used for preprocessing EUS images and machine learning.

There are several limitations to the current project. The first is related to the small sample size; therefore, more studies with more extensive patient data are required to check our results further. Second, we applied stratified fivefold cross-validation to our data, and no real distinct validation datasets were available to assess various methods. Also, our project was performed only in one center, which is the third limitation. Although the operator dependence of EUS

images would reduce when the data are collected from one center, it could be a novel subject to investigate the intraobserver dependency at different centers. Additionally, entering tumor's volume (instead of one slice used in our study) to calculate radiomics features can capture more information about the entire tumor.

Conclusion

Noninvasive ultrasound imaging plays a vital role in the diagnosis of rectal cancer. Speckle noise observed in ultrasound images can affect the image quality and diagnosis; therefore, any method that helps decrease this noise must be utilized. In this regard, many filters and methods have been developed for that purpose. In the current study, the speckle noise reduction was performed using traditional filters, including bilateral, frost, wiener, lee, wavelet, and median filters, compared by different machine learning models. The findings demonstrated that the LR and SVM models had favorable results among the different machine learning methods for the prediction of treatment response. Additionally, among the above-mentioned filters, the wavelet filter had the best performance on the EUS images in rectal cancer based on the radiomics model and PSNR and SSIM parameters.

Supplementary Information The online version contains supplementary material available at https://doi.org/10.1007/s00261-022-03625-y.

Acknowledgements This study was extracted from a Ph.D. thesis from the first author approved by the Tehran University of Medical Sciences. The authors would like to thank the staff of the Medical Imaging and Radiotherapy Oncology centers in Firouzgar Hospital of Iran University of Medical Sciences (Tehran, Iran).

Author contributions SA, HAb, and MA contributed to conceptualization, SA, HAb, and SRM contributed to methodology, SA, HAb, HAr, and SRM contributed to formal analysis and investigation, SA contributed to writing and preparation of the original draft, HAb, HAr, MB, AMA, PF, MA, and SRM contributed to writing, reviewing, and editing of the manuscript, SA, MA, and SRM contributed to funding acquisition, AMA and PF provided resources, MA, SRM, and HAr performed supervision.

Funding This work was supported by the Tehran University of Medical Sciences, under Grant No. 49134.

Declarations

Conflict of interest The authors declare that they have no conflict of interest.

Ethical approval All procedures performed in studies involving human participants were in accordance with the ethical standards of the institutional and/or national research committee and with the 1964 Helsinki Declaration and its later amendments or comparable ethical standards. The study was approved by the Tehran University of Medical Sciences (No. IR.TUMS.MEDICINE.REC.1399.244).

References

1. Chen L-D, Wang W, Xu J-B, et al. Assessment of rectal tumors with shear-wave elastography before surgery: Comparison with endorectal US. Radiology. 2017;285(1):279–292.
2. Chen L Da, Liang JY, Wu H, et al. Multiparametric radiomics improve prediction of lymph node metastasis of rectal cancer compared with conventional radiomics. Life Sci. 2018;208:55–63.
3. Cui Y, Yang X, Shi Z, et al. Radiomics analysis of multiparametric MRI for prediction of pathological complete response to neoadjuvant chemoradiotherapy in locally advanced rectal cancer. Eur Radiol. 2019;29(3):1211–1220.
4. Pizzi AD, Chiarelli AM, Chiacchiaretta P, et al. OPEN MRI - based clinical - radiomics model predicts tumor response before treatment in locally advanced rectal cancer. Sci Rep. 2021;1–11.
5. Chen L-D, Li W, Xian M-F, et al. Preoperative prediction of tumour deposits in rectal cancer by an artificial neural network–based US radiomics model. Eur Radiol. 2020;30(4):1969–1979.
6. Kav T, Bayraktar Y. How useful is rectal endosonography in the staging of rectal cancer? World J Gastroenterol. 2010;16(6):691–697.
7. Sun Q, Lin X, Zhao Y, et al. Deep Learning vs. Radiomics for Predicting Axillary Lymph Node Metastasis of Breast Cancer Using Ultrasound Images: Don't Forget the Peritumoral Region. Front Oncol. 2020;10:1–12.
8. Cusumano D, Dinapoli N, Boldrini L, et al. Fractal-based radiomic approach to predict complete pathological response after chemo-radiotherapy in rectal cancer. Radiol Medica. 2018;123(4):286–295.
9. Karaoğlu O, Bilge HŞ, Uluer İ. Removal of speckle noises from ultrasound images using five different deep learning networks. Eng Sci Technol an Int J. 2021.https://doi.org/10.1016/j.jestch.2021.06.010
10. Singh P, Mukundan R, De Ryke R. Texture based quality analysis of simulated synthetic ultrasound images using local binary patterns. J Imaging. 2018;4(1):1–13.
11. Feng D, Wu W, Li H, Li Q. Speckle noise removal in ultrasound images using a deep convolutional neural network and a specially designed loss function. In: Q. Li et al. (ed) In International Workshop on Multiscale Multimodal Medical Imaging. Springer.Cham. 2019, pp 85–92.
12. Kaur PP, Singh T. Speckle Noise Reduction in Ultrasound Images. NCCI 2010 -National Conference on Computational Instrumentation CSIO Chandigarh. 2010:198–203.
13. Ma X, Shen F, Jia Y, Xia Y, Li Q, Lu J. MRI-based radiomics of rectal cancer: Preoperative assessment of the pathological features. BMC Med Imaging. 2019;19(1):1–7.
14. Shiri I, Hajianfar G, Sohrabi A, et al. Repeatability of radiomic features in magnetic resonance imaging of glioblastoma: Test–retest and image registration analyses. Med Phys. 2020;47:4265–4280.
15. Guiot J, Vaidyanathan A, Deprez L, et al. A review in radiomics: Making personalized medicine a reality via routine imaging. Med Res Rev. 2022;42(1):426–440.
16. Hou M, Sun JH. Emerging applications of radiomics in rectal cancer: State of the art and future perspectives. World J Gastroenterol. 2021;27(25):3802–3814.

17. Wang S, Huang TZ, Zhao X Le, Mei JJ, Huang J. Speckle noise removal in ultrasound images by first- and second-order total variation. Numer Algorithms. 2018;78(2):513–533.
18. Saoji SU, Sarode M V. Speckle and Rician Noise Removal from Medical Images and Ultrasound Images. Int J Recent Technol Eng. 2020;8(5):1851–1854.
19. Duron L, Savatovsky J, Fournier L, Lecler A. Can we use radiomics in ultrasound imaging? Impact of preprocessing on feature repeatability. Diagn Interv Imaging. 2021;102(11):659–667.
20. Loizou CP, Theofanous C, Pantziaris M, Kasparis T. Despeckle filtering software toolbox for ultrasound imaging of the common carotid artery. Comput Methods Programs Biomed. 2014;114(1):109–124.
21. Boldrini L, Cusumano D, Chiloiro G, et al. Delta radiomics for rectal cancer response prediction with hybrid 0.35 T magnetic resonance-guided radiotherapy (MRgRT): a hypothesis-generating study for an innovative personalized medicine approach. Radiol Medica. 2019;124(2):145–153.
22. Delli Pizzi A, Chiarelli AM, Chiacchiaretta P, et al. MRI-based clinical-radiomics model predicts tumor response before treatment in locally advanced rectal cancer. Sci Rep. 2021;11(1):5379-5390.
23. Lovinfosse P, Polus M, Van Daele D, et al. FDG PET/CT radiomics for predicting the outcome of locally advanced rectal cancer. Eur J Nucl Med Mol Imaging. 2018;45(3):365–375.
24. Wang J, Shen L, Zhong H, et al. Radiomics features on radiotherapy treatment planning CT can predict patient survival in locally advanced rectal cancer patients. Sci Rep. 2019;9(1):1–9.
25. Shayesteh SP, Alikhassi A, Farhan F, et al. Author Correction: Prediction of Response to Neoadjuvant Chemoradiotherapy by MRI-Based Machine Learning Texture Analysis in Rectal Cancer Patients. J Gastrointest Cancer. 2020; 51(2):601-609.
26. Vanithamani R, Umamaheswari G. Speckle reduction in ultrasound images using Neighshrink and bilateral filtering. J Comput Sci. 2014;10(4):623–631.
27. Jaybhay J, Shastri R. A Study of Speckle Noise Reduction Filters. Signal Image Process An Int J. 2015;6(3):71–80.
28. Santoso AW, Bayuaji L, Sze LT, Lateh H, Zain JM. Comparison of various speckle noise reduction filters on synthetic aperture radar image. Int J Appl Eng Res. 2016;11(15):8760–8767.
29. Kupidura P. Comparison of filters dedicated to speckle suppression in SAR images. Int Arch Photogramm Remote Sens Spat Inf Sci - ISPRS Arch. 2016;41:269–276.
30. Mohd Sagheer S V., George SN. A review on medical image denoising algorithms. Biomed Signal Process Control. 2020;61:102036.
31. Forman G, Scholz M. Apples-to-Apples in Cross-Validation Studies : Pitfalls in Classifier Performance Measurement. Acm Sigkdd Explorations Newsletter. 2010;12(1):49–57.
32. Berrar D. Cross-Validation Cross-validation. Encyclopedia of Bioinformatics and Computational Biology 2018;1:542–545.
33. Purushotham S, Tripathy BK. Evaluation of Classifier Models Using Stratified Tenfold Cross Validation Techniques. International Conference on Computing and Communication Systems. 2012;680–690.
34. Lee SE, Han K, Kwak JY, Lee E, Kim EK. Radiomics of US texture features in differential diagnosis between triple-negative breast cancer and fibroadenoma. Sci Rep. 2018;8(1):2–9.
35. Liu Z, Zhang XY, Shi YJ, et al. Radiomics analysis for evaluation of pathological complete response to neoadjuvant chemoradiotherapy in locally advanced rectal cancer. Clin Cancer Res. 2017;23(23):7253–7262.
36. Horvat N, Bates DDB, Petkovska I. Novel imaging techniques of rectal cancer: what do radiomics and radiogenomics have to offer? A literature review. Abdom Radiol. 2019;44(11):3764–3774.
37. Huang YQ, Liang CH, He L, et al. Development and validation of a radiomics nomogram for preoperative prediction of lymph node metastasis in colorectal cancer. J Clin Oncol. 2016;34(18):2157–2164.
38. Gillies RJ, Kinahan PE, Hricak H. Radiomics: Images are more than pictures, they are data. Radiology. 2016;278(2):563–577.
39. Chen H, Shi L, Nam K, et al. MRI Radiomics for Prediction of Tumor Response and Downstaging in Rectal Cancer Patients after Preoperative Chemoradiation. Advancesradonc. 2020;5(6):1–10.
40. Jin J, Zhu H, Zhang J, Ai Y, Zhang J, Teng Y. Multiple U-Net-Based Automatic Segmentations and Radiomics Feature Stability on Ultrasound Images for Patients With Ovarian Cancer. Frontiers in Oncology. 2021;18(10):1–8.
41. Zhou H, Jin Y, Dai L, et al. Differential Diagnosis of Benign and Malignant Thyroid Nodules Using Deep Learning Radiomics of Thyroid Ultrasound Images. Eur. J. Radiol. 2020; 127: 108992.
42. Qiu X, Jiang Y, Zhao Q, et al. Could Ultrasound-Based Radiomics Noninvasively Predict Axillary Lymph Node Metastasis in Breast Cancer?," J. Ultrasound Med. 2020; 39(10):1897–1905.
43. Wang Y, Yue W, Li X, et al. Comparison Study of Radiomics and Deep Learning-Based Methods for Thyroid Nodules Classification Using Ultrasound Images. IEEE Access. 2020; 8: 52010–52017.
44. DiCenzo D, Quiaoit K, Fatima K, et al. Quantitative ultrasound radiomics in predicting response to neoadjuvant chemotherapy in patients with locally advanced breast cancer: Results from multi-institutional study," Cancer Med.2020; 9(16):5798–5806.
45. Dasgupta A, Brade S, Sannachi L, et al. Quantitative ultrasound radiomics using texture derivatives in prediction of treatment response to neo-adjuvant chemotherapy for locally advanced breast cancer. Oncotarget. 2020;11(42):3782–3792.
46. Rahman MM, Azim M, Mina, Uddin S. Speckle noise reduction in ultrasound images by wavelet thresholding based on subband mean difference. Int J Tomogr Stat. 2012;20(2):91–97.
47. Bhuiyan MIH, Ahmad MO, Swamy MNS. New spatially adaptive wavelet-based method for the despeckling of medical ultrasound images. Proc - IEEE Int Symp Circuits Syst. 2007;2347–2350.
48. Theek B, Opacic T, Magnuska Z, Lammers T, Kiessling F. Radiomic analysis of contrast-enhanced ultrasound data. Sci Rep. 2018;8(1):1–9.
49. Shayesteh SP, Alikhassi A, Fard Esfahani A, et al. Neo-adjuvant chemoradiotherapy response prediction using MRI based ensemble learning method in rectal cancer patients. Phys Medica. 2019;62:111–119.